Beam Shaping the Direct Laser Interference Patterning Spot

Ludwig Pongratz and Kai Vannahme

Fraunhofer Institute for Laser Technology, Steinbachstrasse 15, 52074 Aachen Germany
Corresponding author's e-mail: ludwig.pongratz@ilt.fraunhofer.de

Direct Laser Interference Patterning (DLIP) using ultrashort pulsed laser sources is a single-step process to produce micro- and nanostructured surfaces by ablation. Spatial periods of a few micrometers are patterned using a laser scanner system with two interfering beams. In this study, the field of DLIP processing is expanded by handling spatial periods in the range of 1 µm and below. Precise periodic ablation is achieved with an optical setup tailored for a homogenous topography of spatial periods in the micro and sub-micrometer range. The lateral intensity distribution of the interference area used for ablation is shaped using beam shapers in order to achieve a homogenous intensity distribution and hence increase the homogeneity of the periodic texture in the ablated area. The shape of the interference area is formed into a square profile for the purpose of seamless stitching plenty of to be processed areas. This creates large area periodic textures with high homogeneity. Two beams with ultrashort laser pulses of 10 ps duration and a wavelength of 532 nm are used to structure line-like periodic surface textures with spatial periods of 650 nm. The beam shaping elements modify the lateral intensity distribution in the interference area and the affiliated profile. This enables precise patterning of tool steels with spatial periods in sub-micrometer range for applications in the field of life science surfaces.

DOI: 10.2961/jlmn.2022.01.2007
Keywords: Direct Laser Interference Pattering DLIP, beam shaping, homogenous topography, large area periodic textures, increase of throughput

1. Introduction

Direct Laser Interference Patterning (DLIP) describes a process for periodic ablation of surface material on micro- and sub-micrometer range where the spatial period is variable. The field of research regarding DLIP spans over varying the wavelength and the pulse duration, using different numbers of partial beams as well as applying hybrid process strategies by using other laser-based patterning processes [1–3]. The state of research is reaching the requirements of industrial applications for line-like and dot-like textures using laser-scanner systems in the micrometer range. The processing speed is increasing and different applications are ready for industrial application, like enhancement of tribological performance or creating anti-icing surfaces [4–6]. In addition to the established research sectors on DLIP, the sub-micrometer range is of interest to life science researchers. The influence of line-like sub-micrometer surface structures on pluripotent stem cells has already been demonstrated using an ns pulse duration. Due to the line-like structure, the stem cells show a preferred growth direction along the sub-micrometer lines [7]. However, the spatial period depends on the incident angle of the superimposed beams. The expression connecting the spatial period, the wavelength and the incident angle for 2-beam interference $\Lambda = \lambda / (2 \sin \alpha)$ [8] is shown for typical laser wavelengths in Fig. 1.

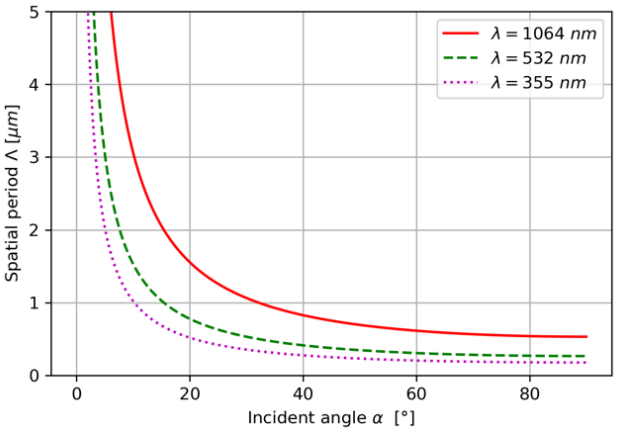

Fig. 1 Connection between angle of incidence α and spatial period Λ for 2-beam DLIP in dependency of the wavelength λ.

Common scanner based spatial periods are bigger than 1.5 µm, which are associated with respective angles of incidences of 6,8° (UV), 10,2° (Green), 20,8° (IR). For spatial periods of 1.5 µm up to 22.2 µm, scanner based DLIP methods reach patterning speeds up to 0.9 m²/min for polycarbonate [1–6, 9].

The research presented in this work is focusing on a 2-beam interference setup using a diffractive optical element (DOE) as beam splitter followed by a reflective prism and a separate adjustable mirror for each partial beam [8]. This setup enables more obtuse angles of incidence and therefore allows to achieve spatial periods smaller than 1.5 µm, e.g. 650 nm. Deterministic patterns on nanometer range are of interest in the field of life science surfaces [7]. In this field, a precise and homogenous periodic topography

with small spatial periods are of interest. For this reason, we developed a setup for an automated variation of the spatial period between 550 nm and 1200 nm [10]. Patterning of areas bigger than the ablation area resulting from a single or multi pulse onto one point is achieved by stitching many ablation areas. Stitching is accompanied by compromises of structural quality in the areas of overlap and/or unpatterned areas depending on the overlap strategy. Remedy can be achieved by forming the beam profile to a square and lateral intensity distribution to be homogenous over its extent. This is the content of this study.

2. Theoretical background

Best topographical results are achieved by single interference spot patterning, also called spot-by-spot patterning. With a common gaussian beam profile, a probe in the working plane can be structured with a high quality of the topography. In comparison, the quality of the topography is reduced in a consecutive overlapping process strategy, which is due to the accumulation of residual heat from multiple pulses at a given position. In addition, transverse vibration of the axis system below the range of the spatial period can negatively affect the topography. The quality of the topography is depending on the process strategy and is illustrated for 1.4301 polished steel in Fig. 2. The interference contrast is optimized by variation of path lengths of the partial beams while measuring the affiliated spot diameter. Both shown results were produced using the same setup and hence the same level of interference contrast.

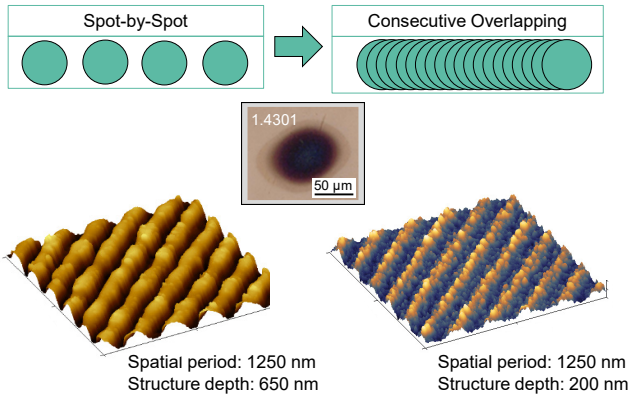

Fig. 2 Process strategies for DLIP: Spot-by-Spot patterning leads to a homogenous topography distribution whereas Consecutive Overlapping results in an inhomogeneous topography distribution with a smaller pattern depth. 1.4301 polished steel. Measurement field size of AFM analysis: 10 x 10 µm²

Due to the elliptic shape of the spot as a result of the inclined superimposed partial beams, area-filling patterning with high structural topography quality is less feasible than using a square interference spot profile. A stitchable spot profile remedy this by lining up the square spots to fill an area. The goal in this study is to shape the beam profile from an elliptic shape to a square shape as well as achieving a homogenous lateral intensity distribution over the whole beam profile. The spot-by-spot method is employed since single spots allow for a precise investigation of the respective profile and the topography. This approach enables large textured areas composed of many stitched spots with high structural topography quality. This non-consecutive approach simplifies the parameter search to optimize topography for different materials since the problems discussed previously do not occur. The spot-by-spot approach is therefore superior when the topographic homogeneity is seen as more important as the process speed. Optimal material-dependent process parameters can be developed in single spot experiments since they are independent of the hatching distance between the spots. This allows for patterning of surfaces with a high topography quality in the sub-micrometer range, which can be applied to polymers by molding, imprinting or embossing.

One approach that has been investigated for beam shaping a 2-beam interference spot is a beam transformation towards a line-like beam profile. This is realized for grating interferometer [11] and transmission prism [12] based interference setups. In both setups, beam shaping is achieved by cylindrical lenses. Thus, the line-shaped spatial beam profiles can increase the throughput for a large-area ablation. An interference tophat beam to generate a square-shaped beam profile was investigated by El-Khoury et al. using a transmission prism-based 4-beam setup. Theoretical calculations and experimental measurements on a CCD Camera confirm a dot-like modulation in a square shaped energy distribution [13]. A comparable approach with a transmission prism-based setup is not possible for lower spatial periods due to the larger incident angle of the partial beams. Hence respective beam shaping elements for each partial beam is necessary.

3. Methods

3.1 Materials

All experiments are conducted on austenitic steel substrates 1.4301 with a thickness of 1 mm. The surface is polished with a surface roughness Ra smaller than 0.3 µm.

3.2 Experimental Setup

The fundamental optical configuration of multi-beam interference patterning setup is 2-beam DLIP. The 2-beam setup using a beam splitter can be designed axisymmetric and requires a minimum number of optical components. Used in connection to an axis system with the ability to trigger a laser in the working plane, pattern sizes in the sub-micrometer range can be patterned with high topographic quality. A Nd:YVO4 slab laser beam source PX100-1-GM (Edge Wave, Wuerselen, Germany) emits a wavelength of 532 nm with a pulse duration of 10 ps and a repetition rate of 100 kHz. The average power can be adjusted by a regulator up to 18 W. The beam is propagating through a focusing lens before split into two partial beams by the beam splitter. The partial beams are reflected by a prism and

mirrors to the working plane, illustrated in Fig. 3.

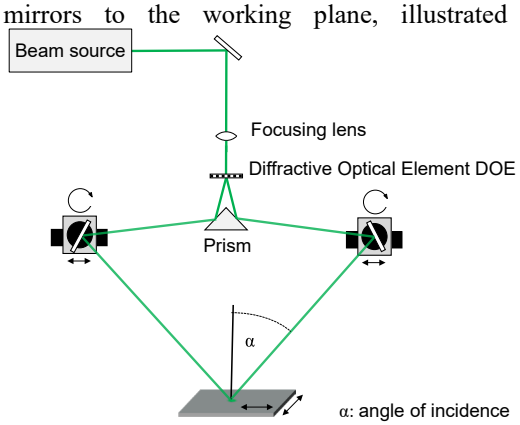

Fig. 3 2-beam DLIP setup in connection to an axis triggered axis laser system for line-like patterns in the nanometer range. The beam is focused by a lens and split by a beamsplitter DOE. Each partial beam is deflected by a prism. Adjustable mirrors guide the partial beams on the working plane.

For reproducible results the interference contrast is maximized. It is the normalized difference of the maximum and minimum values of the periodic intensity modulation. The mirrors are mounted on translation and rotation axis to enable maximizing the interference contrast by minimizing the path difference of the partial beams, which directly impacts the topography quality. The relative quality of the interference contrast can be deduced by comparison of the size of ablation areas for different path length and hence the maximum can be determined. The scalar product of the polarization vectors impacts the interference contrast as a factor too. Consequently, the polarization of the partial beams is adjusted using a wave plate to be perpendicular in the working plane. For a spatial period of 650 nm, the mirrors are guiding the beam in an angle of incidence of 24° onto the working plane. The position of the beam shaping elements (beam profile and lateral intensity distribution) are evaluated by consideration of the results of a beam simulation and the availability on the market. All beam shaping experiments are conducted for a spatial period of 650 nm.

3.3 Beam shaper consideration

Prior to selecting a specific beam shaping element to implement into the setup, the positions in the setup that are considered for implementation are shown schematically in Fig. 4.

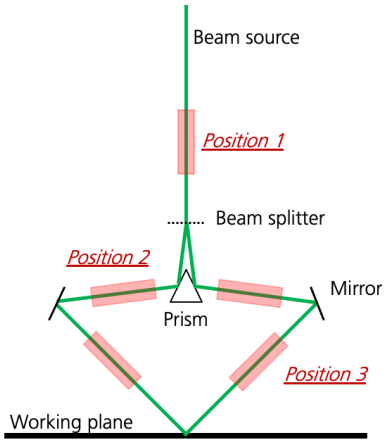

Fig. 4 Schematic setup: Positions for beam shaping elements.

The beam shapers are implemented at position 3 since it is the closest to the working plane and thus the effects of the diffraction limit are minimal. Furthermore, it prevents interactions of the modified beam with subsequent optical components which could affect the quality of the beam shaping. Beam shapers based on phase redistribution are considered to achieve a square beam profile with a tophat intensity distribution in the working plane.

3.4 Simulation model

A simulation study is carried out to examine the potential impact of a phase redistribution beam shaper on the periodic modulation of the intensity distribution. Hence, Visual Studio is used for the simulation due to its wave-optical approach. The experimental setup shown in Fig. 3 is virtually designed without a beam shaper. A beam shaper is separately customized to achieve a tophat intensity distribution for the predefined beam diameter, the distance to the working plane and the desired diameter in the working plane. The local phase redistribution of the virtual beam shaper is shown in Fig. 5 while the resulting intensity distribution on a virtual detector is shown in Fig. 6.

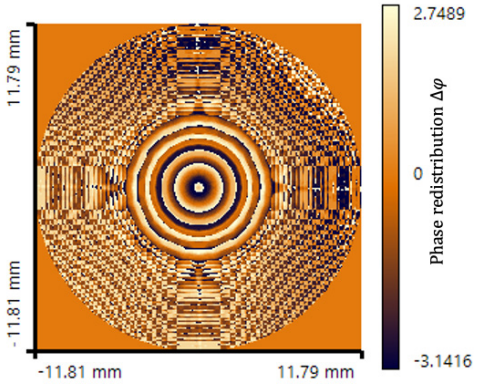

Fig. 5 Local phase redistribution of the beam shaper.

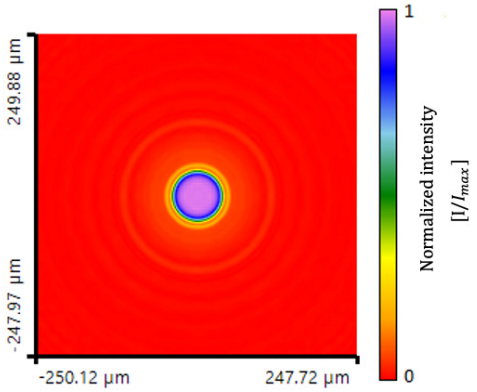

Fig. 6 Intensity distribution resulting from the beam shaper on the virtual detector.

Apart from diffraction effects at the border, the intensity distribution is homogenous. Subsequently, the simulated beam shaper is implemented into the virtual experimental setup at the associated positions (Position 3) in the left and the right partial beam. The resulting intensity distribution in

the working plane of the experimental setup combined with the beam shaper is shown in Fig. 7.

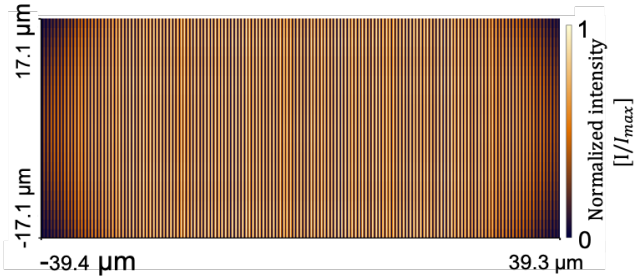

Fig. 7 Cutout of the virtual intensity distribution in the working plane of the experimental setup after implementation of the virtual beam shaper.

Fig. 7 shows a homogenous intensity distribution over the extent of the area of the superimposed partial beams (apart from the desired periodic modulation). The result of the simulation is an indicator that it is possible to use corresponding beam shaping elements for a DLIP setup.

3.5 Beam expander

The beam shaping element which is considered to transform the spatial beam profile and the intensity distribution into a square tophat is the model TH-034-Q-Y-A by the manufacturer Holoor Ltd. Israel. It is optimized to form a 80 µm x 80 µm quadratic spot for beams with a wavelength of 532 nm in a distance of 99.5 mm. It requires a beam profile with a 4σ-diameter of 2.5 mm. Hence, a beam expander is used to adjust the initial diameter of the beam emitted by the beam source to match the requirements. Implementation into the experimental setup is realized at position 1 shown in Fig. 4. The impact of the beam expander on the laser beam is measured at position 3, where the beam shaper is going to be implemented (Table 1). The initial beam diameter has a x-y asymmetry of around 150-200 µm which is propagated by the beam expander. The final diameters in x- and y-direction are adjusted to be symmetric around 2.5 mm so the deviation in both direction is of the same magnitude.

Table 1 Impact of the beam expander on the laser beam measured at the position 3 (Fig. 4), where the beam shaper is implemented.

Position	Axis	ø Before adjustment [mm]	ø After adjustment [mm]	Relative Change [%]
Left beam	X	3.146	2.447	-22.2
	Y	3.007	2.597	-13.6
Right beam	X	3.202	2.467	-23.0
	Y	3.016	2.546	-15.6

After the evaluation of the beam simulation and the availability of beam shaping elements on the market, two identical beam shaping elements of model TH-034-Q-Y-A, are positioned in each partial beam path near the working plane with a focal length of 99.5 mm. In order to feed the correct beam diameter, a lens system was designed. The lens system reduces the input beam diameter from 3.1 mm to 2.5 mm. An input beam diameter of 2.5 mm into the beam shaping elements should lead to a square output beam profile with an edge length of 80 µm.

3.6 Measuring methods

The transformation of the spatial beam profiles of the partial beams by the beam shapers is analyzed using a beam profile camera (Basler acA3800-14µm). Neutral density filters are required to attenuate the power of the partial beams beforehand to a level compatible with the camera. The lateral measurement of the surface structures is carried out using light microscopic images (Keyence VHX7000, Osaka, Japan). Topographic evaluation of the surface structures is performed using atomic force microscopy (AFM, Bruker, USA) by measuring in non-contact mode at a measurement field size of 10 x 10 µm² and a measurement speed of approximately 15 µm/s. The sensitivity of the measuring tip is greater if the measurement is performed transverse to the structure. Therefore, the measurement field is rotated by 45°. 3D images and height profiles are extracted from the obtained topographic AFM data using software (SPIP, Image Metrology A/S, Hørsholm, Denmark). Qualitatively, the occurrence of melt artifacts, which negatively affect the homogeneity of the structure, can be discussed based on the image. These are characterized by z-values deviating from the local average. The spatial period is determined using the mean distance of structure maxima perpendicular to the structure direction for averaged elevation profiles. Structure depth is determined analogously using the mean height difference between adjacent structure minima and structure maxima.

4. Results and discussion

After adapting the beam diameters of left and right partial beams to the required input beam diameter of the beam shaping elements, the spatial beam profile is 75 µm in x-direction and 65 µm in y-direction for the left beam and 72 µm in x-direction and 62 µm in y-direction for the right beam, shown in Fig. 8 and Table 2. The x/y-deviation results from the angle of incidence of 24° (see Fig. 3) at a spatial period of 650 nm, resulting in an elongated x-length. After superimposition of the two shaped partial beams, a rectangle beam profile can be detected in the working plane. The beam profile in x/y-direction of the superimposed tophat is 73/64 µm. The spatial profile resembles a square, with the upper right corner less pronounced. This can be traced back to the spatial profile of the right beam. Since both beam shaping elements have to be adjusted precisely onto the same point, deviations from the optimum may occur because the second beam shaping element is adjusted onto the

optimum of the first.

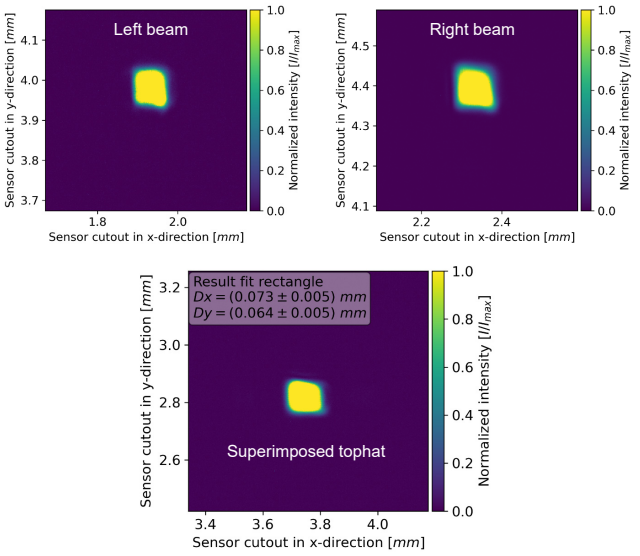

Fig. 8 Tophat beam profile of each partial beam and the superimposed beam profile in the working plane.

After superimposition of the shaped partial beams, a maximum relative change in the beam profile of 3.2% can be measured. The beam profile of the superimposed tophat decreases compared to the left partial beam and increases compared to the right partial beam, shown in Table 2.

Table 2 Dimensions of the tophat beam profile of each partial beam and the superimposed beam profile in the working plane.

Position	Axis	ø Before superimpo. [µm]	ø After superimpo. [µm]	Relative Change [%]
Left beam	X	75	73	-2.7
	Y	65	64	-1.5
Right beam	X	72	73	+1.4
	Y	62	64	+3.2

The gaussian beam profile, resulting from the standard DLIP setup without beam shapers, is larger than the tophat beam profile. The oval shape of the gaussian beam profile has 4σ-diameter of 242 µm in x-direction and 188 µm in y-direction, shown in Fig. 9 in comparison to the tophat beam profile. The elongated x-length is also based on the angle of incidence of 24° (see Fig. 3). The smaller spot area of the shaped tophat results from the higher focusing of the beam shapers.

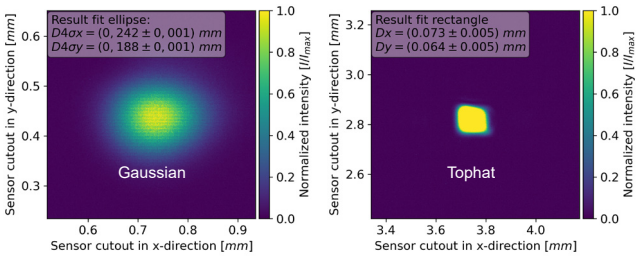

Fig. 9 Superimposed beam profiles of an unshaped gaussian and a shaped tophat spot in the working plane.

The area in the working plane of the gaussian beam is 0.0357 mm². The area of the tophat beam is 0.0046 mm². Thus, after beam shaping, the area is about 8 times smaller. The relative length change in x/y-direction from gaussian to tophat is -69.8/-66.0%, listed in Table 3.

Table 3 Dimensions of the superimposed beam profiles of an unshaped gaussian and a shaped tophat spot in the working plane.

Position	Axis	ø Gaussian [µm]	ø Tophat. [µm]	Relative Change [%]
Working plane	X	242	73	-69.8
	Y	188	64	-66.0

In consequence, a smaller ablated spot diameter on a workpiece can be expected, while the fluence for the shaped spot is increased. First patterning experiments on polished steel plates are shown in Fig. 10. Both spots were patterned using 3 pulses at a pulse energy of 29.7 µJ. The fluences per pulse for gaussian and tophat spots are 83 mJcm^{-2} and 636 mJcm^{-2}. In this case, the fluence for the tophat beam is 8 times higher. According to the measured beam profiles, the patterned areas on a steel plate are shown in Fig. 10.

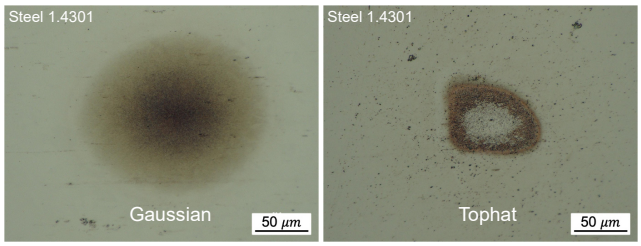

Fig. 10 Patterned areas on a steel plate 1.4301 using the superimposed gaussian and tophat beam profile. The spots are patterned using 3 pulses at a pulse energy of 29.7 µJ. The fluence per pulse for gaussian spot is 83 mJcm^{-2} and 636 mJcm^{-2} for the tophat spot.

The patterned area is measured using the light microscope and is defined by the visible borders of the ablated areas. The respective maximum values in x- and y-direction represent the measurement results. The patterned area using the gaussian beam profile is 1.2 times smaller than the corresponding beam profile. The patterned area using the tophat beam profile is 1.1 times larger than the corresponding beam profile. It is visible, that the diminished upper right corner carried over to the patterned area. The fluence per pulse in dependency of the pulse energy for gaussian and tophat spots are illustrated in Fig. 11. The linear increase of the fluence per pulse for the tophat beam profile is higher than the gaussian beam profile. The gradient for the tophat is 21.4 mJcm^{-2} (µJ)$^{-1}$ and 2.8 mJcm^{-2} (µJ)$^{-1}$ for the gaussian beam profile. A result of the higher fluence per pulse for the tophat beam profile is the absence of periodic structure in the center of the respective ablated area (Fig. 10). It is destroyed by accumulated residual energy.

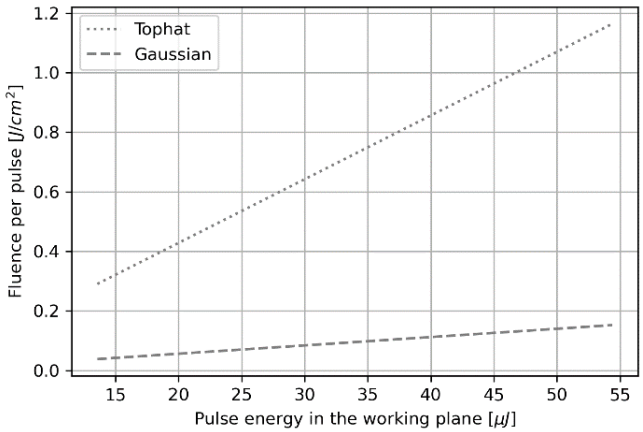

Fig. 11 Fluence per pulse in dependency of the pulse energy for gaussian and tophat spots in the working plane.

Furthermore, the correlation between patterned spot diameter in y-direction and fluence per pulse for the gaussian (Fig. 12) and the tophat beam profile (Fig. 13) can be plotted. It should allow conclusions on the respective lateral intensity distribution. Measurements of the diameters follow the previously described procedure. The fluence spectrum for the gaussian spot reaches 38.0 mJcm^{-2} to 152.2 mJcm^{-2}, which has an approximately 8 times smaller range than the fluence spectrum of the tophat spot. The tophat fluence ranges between 290.4 mJcm^{-2} to 1164.0 mJcm^{-2}. For both beam profiles, the diameters of the patterned areas increase with a rising fluence.

The diameter for the gaussian beam profile in y-direction is 188 µm, based on the 2σ-limit. The region beyond this limit represents a small part (4.6%) of the total energy of a pulse. With increasing pulse energies, the increase of the local fluence outside the 2σ-limit is smaller than inside the limit. Therefore, the increase in diameter stagnates for diameters approaching the limit (188 µm), shown in Fig. 12.

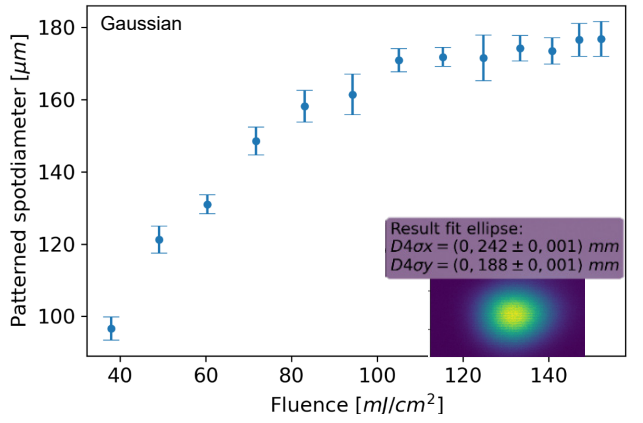

Fig. 12 Patterned spot diameter in y-direction and fluence per pulse for the gaussian spot.

The diameter in y-direction for the tophat beam profile is 64 µm. The edges of the beam profile are steep compared to the gaussian beam profile. Thus, the corresponding diameter also increases linearly as the fluence increases. The stagnation of the diameters in the upper fluence region results from exceeding the diameter of the beam profile in contrast to the gaussian beam profile, shown in Fig. 13.

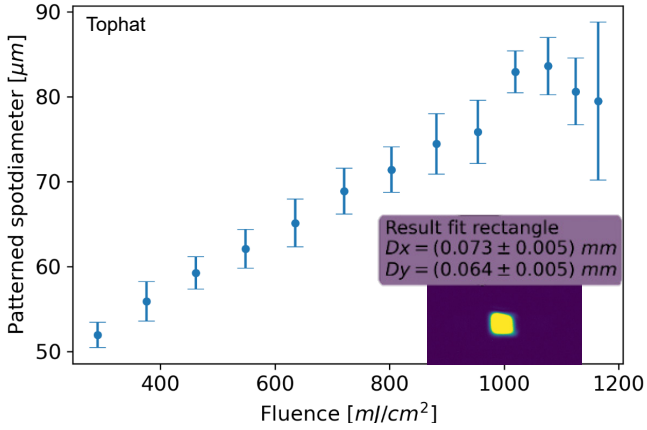

Fig. 13 Patterned spot diameter in y-direction and fluence per pulse for the tophat spot.

A homogenous patterning over the whole tophat spot can be detected for a 1 pulse spot, patterned at the lower limit of the tophat fluence spectrum at 290.4 mJcm^{-2} (Fig. 14). The patterned area has a homogenous coloration, which indicates a homogenous intensity distribution as well. Patterned areas using an unshaped gaussian spot (see Fig. 10) have different zones of coloration and thus, different topography characteristics and quality. Accordingly, under-structured areas without patterns occur at the edges of a DLIP spot. In the center of a DLIP spot, over-structured areas can emerge resulting in topography deformations induced by heat overflow. A validation of the topography characteristics for the beam shaped tophat spot is done by AFM analyses of an edge, intermediate and center area. These different areas are marked in Fig. 14.

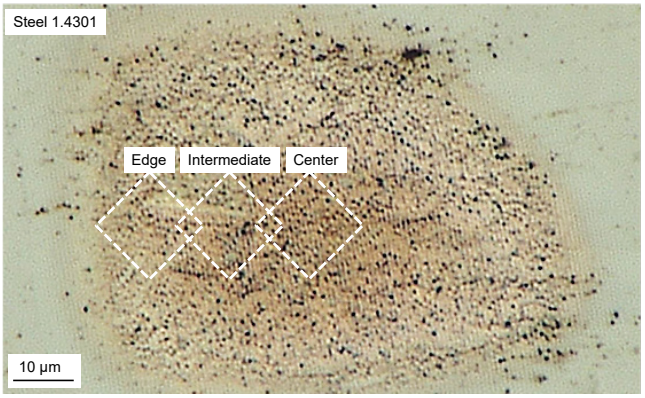

Fig. 14 Patterned area using a tophat spot and 1 pulse at the lower limit of the fluence regime (290.4 mJcm^{-2}). An edge, intermediate and center area is marked for AFM analyses.

In Fig. 14, black residues can be seen over the whole patterned area. It can also be seen in the region around a patterned spot, as shown in Fig. 10. Further investigation with respect to these residues needs to be performed. Therefore, a fluence lower than the lower limit of the tophat fluence spectrum has to be carried out by integrating a beam attenuation in future experiments.

The AFM analyses of the edge, intermediate and center area of the patterned spot in Fig. 14 is shown in Fig. 15. The line-like patterns have homogenous characteristic in all investigated areas. The topography distribution is constant. Melting beads in all areas indicate that a lower fluence could

yield even better structuring results. Another indication that further investigations must be carried out using a fluence lower than 290.4 mJcm^{-2}.

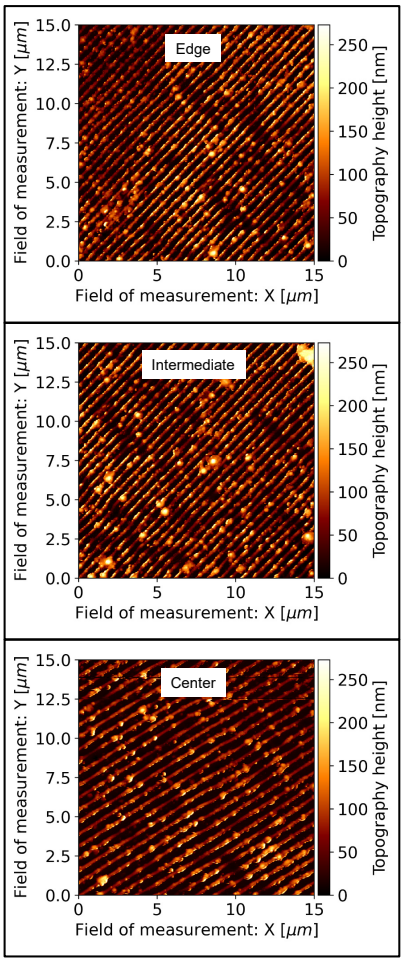

Fig. 15 AFM analyses of the line-like pattern in the center, intermediate and edge area. Analysis area: 15 µm x 15 µm.

To evaluate the homogeneity characteristics over a whole spot, the aspect ratio is a suitable evaluation factor. Based on AFM analyses, the aspect ratio indicates different topography areas known from DLIP pattering using gaussian spots and the occurrence of heat effected artifacts like melting beads. The aspect ratio for the center, intermediate and edge area is plotted in Fig. 16. It is nearly constant at 0.2 µm.

Fig. 16 Aspect ratio of the edge, intermediate and center area for line-like patterns. An indication for a homogenous intensity distribution over the whole tophat spot.

5. Summary

In this study, the application of beam shaping elements for a 2-beam DLIP setup using an ultrashort pulsed laser source can be confirmed. At a pulse duration of 10 ps and a wavelength of 532 nm, line-like patterns with a spatial period of 650 nm are patterned on stainless steel. A simulation model is used to investigate the feasibility of diffractive optic elements as beam shapers in a DLIP setup. Furthermore, advantages and disadvantages of different positions of the beam shapers are considered. After implementation of beam shaping elements based on phase redistribution, an unshaped gaussian beam profile is compared to a shaped tophat beam profile. The fluence in the working plane for the tophat spot is approximately 8 times higher than for the gaussian spot. This is due to the focusing function of the implemented beam shaping elements. Consequently, an area is patterned using 1 pulse of the tophat beam profile at the lower limit of the fluence spectrum (290.4 mJcm^{-2}). The patterned area has a more homogenous topography distribution compared to the patterned area using a native gaussian beam profile. The aspect ratio in the edge, intermediate and center area of this spot is nearly constant at 0.2 µm. Thus, a homogeneous topography distribution across a beam shaped interference spot is feasible. This is a step towards an area-filling patterning with high structural topography quality. Difficulties which arose during the study mainly concerned the adjustment of the two beam shaping elements onto each other. It requires the setup to be more precisely adjusted than for periodic ablation without beam shaper. The beam shapers themselves have to be meticulously positioned such that a good overlap of the two shaped partial beams is achieved. An approach to solve this might be to instead position a single beam shaper into the setup before the beamsplitter. After positioning the beam shapers, the overall stability of the setup is long time stable.

6. Outlook

New parameter studies with fluences lower than lower limit in this study have to be carried out by implementing a beam attenuation. Thus, a topography without thermal artifacts can be achieved. After showing the successful implementation of beam shaping elements, a stitching of beam shaped tophat spots has to be executed for an efficient area packing while achieving a homogenous topography. Using a spot-by-spot process strategy and a homogenous intensity over the tophat spot area, an extended patterned area has to be patterned. The throughput compared to DLIP patterning without tophat should be increased like El-Khoury et al. presented in a further study on DLIP beam shaping in 2022 [14].

7. Acknowledgment

This work is funded by the German Research Foundation (DFG; GI 265/22-1) within the Project “TopoStem - The influence of sub-µm surface structures on pluripotent stem cells”.

8. References

[1] M. Soldera, S. Alamri, P. A. Sürmann, T. Kunze, and A. F. Lasagni: Nanomaterials, 11, (2021) 129.

[2] M. Mezera, S. Alamri, W. Hendriks, A. Hertwig, A. M. Elert, J. Bonse, T. Kunze, A. F. Lasagni, and G. Römer: Nanomaterials, 10, (2020), 1184.
[3] F. Kuisat, F. Ränke, F. Lasagni, and A. F. Lasagni: Materials, 14, (2021), 2563.
[4] T. Stark, S. Alamri, A. Aguilar-Morales, T. Kiedrowski, and A. F. Lasagni: J. Laser Micro Nanoeng., 14, (2019), 13.
[5] V. Vercillo, S. Tonnicchia, J. Romano, A. Garcia-Giron, A. Aguilar-Morales, I. Alfredo, and S. Alamri: Adv. Funct. Mater., 30, (2020), 1910268.
[6] S. Alamri, B. Krupop, T. Steege, A. Aguilar-Morales, V. Lang, S. Storm, F. Schell, C. Zwahr, C. Kracht, M. Bieda, B. Voisiat, U. Klotzbach, A. F. Lasagni and T. Kunze: SPIE Proc. Vol. 10906, (2019) 109060S.
[7] G. Abagnale, A. Sechi, M. Steger, Q. Zhou, C. Kuo, G. Aydin, C. Schalla, G. Müller-Newen, M. Zenke, I. G. Costa, P. van Rijn, A. Gillner and W. Wagner: Stem Cell Rep., 9, (2017), 654.
[8] M. Steger and A. Gillner: J. Laser Micro Nanoeng., 11, (2016), 296.
[9] V. Lang, T. Roch, and A. F. Lasagni: Adv. Funct. Mater., 18, (2016), 1342.
[10] L. Pongratz and K. Vannahme: SPIE Proc. Vol. 11674, (2021) 116740P.
[11] J.-H. Klein-Wiele, J. Bekesi, J. Ihlemann, and P. Simon: SPIE Proc. Vol. 8796, (2013) 87962H.
[12] V. Lang, B. Voisiat, T. Kunze, and A. F. Lasagni: Adv. Funct. Mater., 21, (2019), 1900151.
[13] M. El-Khoury, B. Voisiat, T. Kunze, and A. F. Lasagni: J. Laser Micro Nanoeng., 13, (2018), 268.
[14] M. El-Khoury, B. Voisiat, T. Kunze, and A. F. Lasagni: Materials, 15, (2021), 2563.

(Received: July 28, 2021, Accepted: July 23, 2022)